DALTON
FULL PAPER

Synthesis, X-ray structure and molecular modelling analysis of cobalt(II), nickel(II), zinc(II) and cadmium(II) complexes of the widely used anti-inflammatory drug meloxicam †

Sandra Defazio and Renzo Cini *

Department of Chemical and Biosystem Sciences and Technologies, University of Siena, Via A. Moro 2, I-53100 Siena, Italy. E-mail: cini@unisi.it

Received 21st August 2001, Accepted 6th February 2002
First published as an Advance Article on the web 10th April 2002

The reactions of cobalt(II)-, nickel(II)-, zinc(II)- and cadmium(II)-acetates with the widely used anti-inflammatory drug meloxicam (H_2mel, 4-hydroxy-2-methyl-*N*-(5-methyl-2-thiazolyl)-2*H*-1,2-benzothiazine-3-carboxamide-1,1dioxide) in methanol produced micro-crystalline solids which were collected and recrystallized from dimethylsulfoxide (dmso) solution to give crystals of *trans*,*trans*-[M^{II}(Hmel)$_2$(*O*-dmso)$_2$] (M = Co, **1**; Ni, **2**; Zn, **3**; Cd, **4**). The X-ray diffraction analyses showed that **1**, **3** and **4** are isomorphous and isostructural. The two $Hmel^-$ anions chelate the metal centre through the nitrogen atom from the thiazole ring and the amide oxygen atom at the equatorial positions, whereas the two dmso molecules link the metal at the apical sites through their oxygen atoms. The metal atom is pseudo-octahedrally co-ordinated, the M–O(amide) bond distances being 2.083(3), 2.081(4) and 2.269(2) Å, and the M–N(thiazole) lengths 2.088(3), 2.060(4) and 2.254(2) Å for **1**, **3** and **4**, respectively. The $Hmel^-$ ligand adopts a *ZZZ*-conformation which is stabilised by a strong intramolecular O ··· H–N hydrogen bond and the conformation of the thiazine ring changes from a half-chair to an envelope. The ^{1}H NMR spectrum for **3** (298 K) shows well defined peaks, and the H(N) amide and H(thiazole ring) proton signals (9.66 and 7.43 ppm) experience significant effects upon deprotonation and metal ligation. The quantum mechanics semi-empirical ZINDO/1 method reproduces the structures of the ligand molecules (H_2mel and $Hmel^-$) at an acceptable degree of accuracy except for the S–O bond distances. The computed complex-formation enthalpies at the gas phase for the model metal-chelates $M^{II}(^-$O–CH=CH–C(=*O*)NH–(ring-**C**=*N*–CH=CH–**S**))$^+$ (M = Co, Ni, Cu, Zn) are in the range −2711–−3228 kJ, much lower than the enthalpy of protonation of $Hmel^-$ (−2094 kJ). The computed complex-formation enthalpy for the Cd(II)-chelate (−2158 kJ) is close to the enthalpy of protonation of $Hmel^-$. The computed spectrum for Zn($^-$O–CH=CH–C(=*O*)NH–(ring-**C**=*N*–CH=CH–**S**))$_2$ has an intense effect only in the region 300–400 nm attributable to HOMO–LUMO + 1 or thiazole-to-enol charge transfer. The geometry optimisations at the density functional Becke3LYP/(Lanl2dz; 6-31G**, S) level reproduce very well the structures of H_2mel and the M($^-$O–CH=CH–C(=*O*)NH–(ring-**C**=*N*–CH=CH–**S**))$_2$ (M = Zn, Cd) moieties of **3** and **4**, and produce a reliable structure for Cu($^-$O–CH=CH–C(=*O*)NH–(ring-**C**=*N*–CH=CH–**S**))$_2$. The complex molecules **1**, **3** and **4** as well as the model bis-chelates are highly hydrophobic in the exterior surface; this suggests a facile cell membrane permeability and an inertness towards dissociation in aqueous media for the potential anti-inflammatory drugs **1** and **3**.

Introduction

Metal complexes containing non-steroidal anti-inflammatory drugs (NSAIDs; see Scheme 1 for the molecular formulae of selected drugs from the "oxicam" family) are among those compounds which have received much attention and increasing interest from a medicinal inorganic chemistry viewpoint,[1,2] in the field of co-ordination compounds with active drugs as ligands, during the last decade.[3–9] The case of indomethacin and its metal complexes can be considered as a typical example of how much the co-ordination compounds of certain metals can improve the overall quality of the drug by reducing the damaging effects on the gastro-intestinal system and increasing the anti-inflammatory action, when compared to the uncomplexed drug. Certain metal complexes of indomethacin are now being prepared in millions of doses as veterinary pharmaceuticals (see ref. 3*a* and references therein). Metal complexes of anti-inflammatory drugs can also be potentially active against other diseases such as cancer and bacterial infections, as is the case when the co-ordination residues contain metals like Pt(II), Pt(IV), Ru(II), Ru(III), Rh(II), Rh(III), Ag(I), Au(I), *etc.*[3,4,10–14]

It has been reported that meloxicam (Mobic, Boehringer-Ingelheim) has a good selectivity profile as regards the inhibition of the cyclo-oxygenase (COX) activity of prostaglandin endoperoxide synthase, the inhibition of the COX2 isoform being required to decrease the inflammatory processes, whereas the inhibition of the COX1 isoform causes gastro-intestinal and renal toxicity.[15] For this reason meloxicam is actually one of the most widely administered NSAIDs against the symptoms of osteoarthrosis and chronic polyarthritis. It is commonly accepted by the community of medicinal chemists that a deep knowledge of the chemical structure and the physico-chemical properties of metal-active drug compounds is preliminary to the investigation of their pharmaceutical activity.[3*a*] NSAIDs from the "oxicam" family have several potential donors towards metal ions, and at least three different co-ordination modes have been found for piroxicam (H_2pir) in the solid state *via* X-ray diffraction.[6*a*,8] H_2pir reacts as a singly deprotonated chelating ligand *via* pyridyl nitrogen and amide oxygen towards Cu(II) and Cd(II),[8*a*] as a mono-dentate ligand *via* pyridyl nitrogen towards Pt(II),[8*b*,*c*] and as a di-anionic tri-dentate ligand *via* amide oxygen and nitrogen, and pyridyl nitrogen towards Sn(IV).[6*a*] It is therefore worth investigating the co-ordinating

† Electronic supplementary information (ESI) available: crystallographic data, atomic co-ordinates and thermal and geometrical parameters for **1**, **3** and **4**; pictures of the electrostatic potential surfaces for selected molecules. See http://www.rsc.org/suppdata/dt/b1/b107594m/

 DOI: 10.1039/b107594m

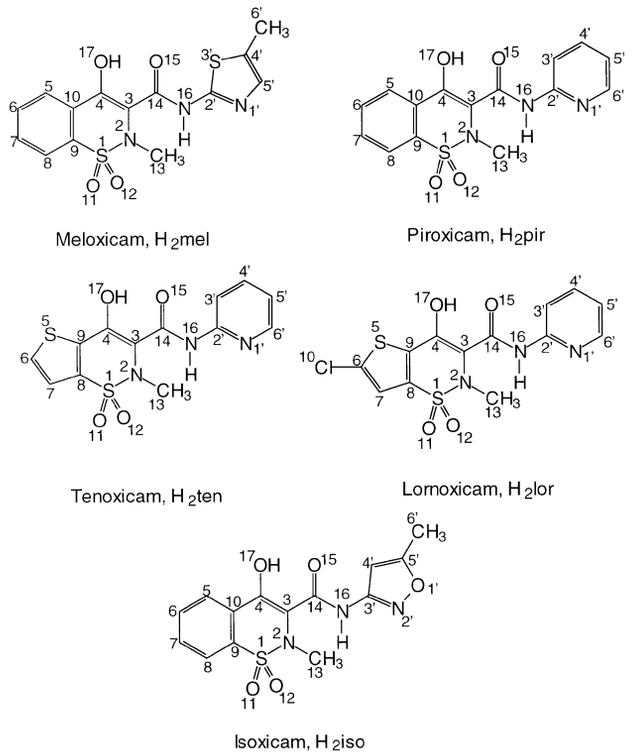

Scheme 1 Structural formulae for selected non-steroidal anti-inflammatory drugs (NSAIDs) from the oxicam family. The numbering of the atoms used throughout the paper is also reported. All the molecules have the 17,1′-*EZE*-conformation.

ability of other NSAIDs from the "oxicam" family. The search for molecular modelling tools to gain an insight into the structure of co-ordination molecules and metal complex–biomolecule systems is a fast expanding area because of the advances in bio-co-ordination and medicinal inorganic chemistry as well as in computers and computational methods.[16,17] Molecular mechanics, semi-empirical quantum mechanics, density functional and *ab initio* quantum mechanics methods can be used to investigate a large variety of structural, electronic, spectroscopic and thermodynamic properties at different degrees of accuracy, depending on the size of the system investigated, on the power of the computer and program capabilities. Several possible choices of method and computer programs are available to most inorganic chemistry laboratories; the selection of the optimal computational strategy for each type of complex molecule is often crucial.

On the basis of this reasoning, the synthesis and the X-ray structural characterisation of metal complexes of meloxicam have been performed in this laboratory as a continuation of a research project started here some twelve years ago with the isolation and the structural characterisation of the first series of co-ordination compounds of piroxicam.[8a] The meloxicam complexes have been here characterised also for their spectroscopic (IR, UV, ^{1}H NMR) properties. A molecular modelling analysis through the techniques of molecular mechanics, semi-empirical quantum mechanics and density functional theory has been carried out on the selected ligands and their metal complex molecules. We wish to report here on the results of the work relevant to compounds **1**–**4**.

Experimental

Materials

$Co(CH_3COO)_2\cdot 4H_2O$ (Riedel-De Haen), $Ni(CH_3COO)_2\cdot 4H_2O$ (Merck), $Zn(CH_3COO)_2\cdot 2H_2O$ (Erba), $Cd(CH_3COO)_2\cdot 2H_2O$ (Erba) and meloxicam (Boehringer-Ingelheim) were used as purchased without any further purification. Dmso (analytical grade, a. g., BDH), ethanol 99% (EtOH, a. g., Baker), methanol (MeOH, a. g., Baker) and diethyl ether (Et_2O, a. g., Baker) were also used without any further purification.

Synthesis of *trans*,*trans*-[M^{II}(Hmel)$_2$(*O*-dmso)$_2$], M = Co, 1; Ni, 2; Zn, 3; and Cd, 4. The complexes were prepared according to the following procedure. Meloxicam (0.088 g, 0.25 mmol) and $M^{II}(CH_3COO)_2$ (0.125 mmol) were dissolved separately in hot MeOH (50 cm^3 and 5 cm^3, respectively). The two clear solutions were mixed and the final mixture was refluxed under stirring for *ca.* 0.5 h. The complexes precipitated as microcrystalline powders after a few minutes of mixing. The solid compounds were filtered, washed with hot MeOH, and then dried under vacuum at 298 K. The crude products were re-crystallised from dmso. The Co(II), Ni(II), Zn(II) and Cd(II) derivatives gave pale orange, pale green, yellow and yellow crystals, respectively. Yields 60–88%. The analytical data are in agreement with the formula [M(Hmel)$_2$(*O*-dmso)$_2$]. Anal. Calcd. for $C_{32}H_{36}CoN_6O_{10}S_6$ (MW = 915.96), **1**: C, 41.96; H, 3.96; N, 9.17; S, 21.00. Found: C, 41.99; H, 4.21; N, 8.98; S, 21.18%. Calcd. for $C_{32}H_{36}N_6NiO_{10}S_6$ (MW = 915.77), **2**: C, 41.97; H, 3.96; N, 9.18; S, 21.01. Found: C, 41.86; H, 4.08; N, 8.86; S, 21.36%. Calcd. for $C_{32}H_{36}N_6O_{10}S_6Zn$ (MW = 922.40), **3**: C, 41.31; H, 4.04; N, 8.97; S, 20.92. Found: C, 41.66; H, 3.93; N, 9.11; S, 20.86%. Calcd. for $C_{32}H_{36}CdN_6O_{10}S_6$ (MW = 969.43), **4**: C, 41.31; H, 4.04; N, 8.97; S, 20.92. Found: C, 41.66; H, 3.93; N, 9.11; S, 20.86%. UV (7.0×10^{-5} mol dm^{-3} in $CHCl_3$): 370 nm (ε/ 25000 cm^{-1} mol^{-1} dm^3, **1**), 374 nm (31000, **2**), 374 nm (35700, **3**), 348 nm (32700, **4**), and 343 nm (19700, H_2mel).

X-Ray crystallography

Data collection. The data collection for the well formed crystals of **1**, **3** and **4** was performed using a Siemens P4 automatic four circle diffractometer operating at 295 ± 2 K with graphite monochromated Mo-Kα radiation (λ = 0.71073 Å). Preliminary investigations performed using the Weissenberg techniques showed that the crystals belong to the triclinic system. Accurate cell constant determinations were obtained *via* the least-squares method applied to the values of several (36, 20, 22) randomly selected strong reflections measured *via* the automatic diffractometer. The intensities were corrected for Lorentz-polarisation effects, and absorption effects (*via* the ψ-scan technique based on at least three reflections) by using the XSCANS[18] and XEMP[19] packages. Selected crystallographic data are listed in Table 1.

Structure solution and refinement. The structure solutions for **1**, **3** and **4** were performed by locating the metal atom at an inversion centre of 0,0,0 and computing subsequent difference-Fourier maps and least-squares cycles. All the non-hydrogen atoms were easily located through this procedure whereas all the hydrogen atoms were located through the HFIX and AFIX options of SHELXL-97.[20] The non-hydrogen atoms were refined as anisotropic whereas the hydrogen atoms were treated as isotropic. The calculations relevant to the structure refinements were performed using the SHELXL-97 package, whereas the molecular geometries and the molecular graphics were computed by using the PARST-97,[21] ORTEP-3[22] and XPMA-ZORTEP packages.[23] The machines used were Pentium personal computers.

CCDC reference numbers 169593–169595.

See http://www.rsc.org/suppdata/dt/b1/b107594m/ for crystallographic data in CIF or other electronic format.

Spectroscopy

The IR spectra were recorded by using the nujol mull and KBr pellet techniques and a Perkin-Elmer model 1600 Fourier-transform spectrometer. UV spectra were recorded by using a

Table 1 Crystal data and structure refinement for $[Co(Hmel)_2(O\text{-dmso})_2]$, **1**, $[Zn(Hmel)_2(O\text{-dmso})_2]$, **3**, and $[Cd(Hmel)_2(O\text{-dmso})_2]$, **4**

Parameter	**1**	**3**	**4**
Empirical formula	$C_{32}H_{36}CoN_6O_{10}S_6$	$C_{32}H_{36}N_6O_{10}S_6Zn$	$C_{32}H_{36}CdN_6O_{10}S_6$
Formula weight	915.96	922.40	969.43
Crystal system	Triclinic	Triclinic	Triclinic
Space group	$P\bar{1}$	$P\bar{1}$	$P\bar{1}$
Unit cell dimensions			
a/Å	7.844(1)	7.878(4)	7.978(1)
b/Å	9.153(3)	9.127(6)	9.413(4)
c/Å	13.914(1)	13.873(7)	13.766(1)
α/°	79.12(1)	79.26(4)	78.72(1)
β/°	85.74(1)	85.90(3)	86.35(1)
γ/°	81.87(1)	81.67(4)	82.56(2)
Volume/Å^3	970.0(3)	968.7(9)	1004.5(5)
Z	1	1	1
Calculated density/Mg m^{-3}	1.568	1.581	1.603
Reflections collected/unique	4223/3413 [R(int) = 0.0274]	3650/3393 [R(int) = 0.0619]	3802/3528 [R(int) = 0.0088]
Absorption correction	ψ-scan	ψ-scan	ψ-scan
Refinement method	Full-matrix least-squares on F^2	Full-matrix least-squares on F^2	Full-matrix least-squares on F^2
Data/restraints/parameters	3413/0/250	3393/0/250	3528/0/250
Final R indices [$I > 2\sigma(I)$]	$R1$ = 0.0499, $wR2$ = 0.1050	$R1$ = 0.0603, $wR2$ = 0.1361	$R1$ = 0.0267, $wR2$ = 0.0735
R indices (all data)	$R1$ = 0.0832, $wR2$ = 0.1192	$R1$ = 0.1040, $wR2$ = 0.1600	$R1$ = 0.0307, $wR2$ = 0.0763

Perkin-Elmer EZ-201 spectrophotometer. ^{1}H NMR spectra were recorded using Bruker AC-200 and Bruker 600 spectrometers.

Molecular modelling

Molecular mechanics. The molecular mechanics calculations were performed by using the MacroModel (MMOD) version 5.0 package[24] and a Silicon Graphics Indigo 2 computer. The molecules investigated were *EZE*-, *EZZ*- and *ZZZ*-H_2mel (see Schemes 1 and 2 for selected forms and conformations), and *trans*-$Zn(Hmel)_2$ (a planar arrangement of the co-ordination sphere atoms was used for the bis-chelate). The strain energies were computed by taking into account the bond stretching (E_b), bond bending (E_θ), bond torsion (E_ϕ), non-bonding (E_{nb}) and hydrogen bonding (E_{hb}) contributions. The force field employed is an AMBER[25] type one based on the parameters implemented in the MMOD package (as regards the ligand molecules) as properly adapted for the interactions which involve the co-ordination sphere atoms. The new force field parameters were refined to obtain better agreement between the computed and the experimental (solid state, X-ray diffraction) geometrical parameters.

Semi-empirical methods. All the calculations were performed using the HyperChem 5.1 package.[26] The molecular structures for *EZE*-H_2mel, *ZZZ*-H_2mel, *EZZ*-H_2mel, *ZZE*-H_2mel, zwitterionic *ZZZ*-H_2mel^{+-}, *ZZZ*-H_2pir^{+-}, cationic *EZZ*-H_3mel^+, anionic *EZZ*-$Hmel^-$, *ZZE*-$Hmel^-$, $(MOD\text{-}B)^-$ (Scheme 3), $(MOD\text{-}C)^-$, $(MOD\text{-}D)^-$, $(MOD\text{-}E)^-$, $Zn(MOD\text{-}C)^+$, $Zn(MOD\text{-}E)^+$, $Cd(MOD\text{-}C)^+$, $Cu(MOD\text{-}C)^+$ (doublet, uhf), $Ni(MOD\text{-}C)^+$ (triplet, uhf), $Co(MOD\text{-}C)^+$ (quartet, uhf) and $Zn(MOD\text{-}C)_2$ were optimised in the gas phase by using the ZINDO/1 level of approximation[27] and the restricted Hartree–Fock wave function, rhf, unless specified for the unrestricted Hartree–Fock function, uhf, (see ref. 26, and references therein). The convergence criterion for the geometry optimisation was 0.042 kJ mol^{-1} for all the molecules except for $Zn(MOD\text{-}C)_2$ (0.105 kJ mol^{-1}). The molecules were usually fully optimised without any restraint with the exception of $Zn(MOD\text{-}C)^+$, $Zn(MOD\text{-}E)^+$, $Cd(MOD\text{-}C)^+$, $Cu(MOD\text{-}C)^+$, $Ni(MOD\text{-}C)^+$, $Co(MOD\text{-}C)^+$ and $Zn(MOD\text{-}C)_2$ for which the following bond and torsion angles were restrained to the values taken from the corresponding solid state structures with $Hmel^-$ as the ligand or chosen to fix the planarity of certain moieties: O(15)–M–N(1′) (force constant 41858.0 kJ), N(16)–C(2′)–S(3′) (4185.8), M–N(1′)–C(5′) (4185.8), N(16)–C(14)–O(15)–M (0°, 41858.0), N(16)–C(2′)–N(1′)–M (0°, 41858), and, for $Zn(MOD\text{-}C)_2$ only, C(14)–O(15)–Zn–N(1′B) (180°, 4185.8). The structural data for the restraints on $Ni(MOD\text{-}C)^+$ were those of **3**, whereas the data of Cu(II)–piroxicam[8a] were used for the restraints on $Zn(MOD\text{-}E)^+$. The UV spectra were computed by using single point calculations at the ZINDO/S[28] singly excited interaction configuration level on the molecules previously optimised through the ZINDO/1 method. The σ–σ and π–π overlap weighting factors were those implemented in the program.[26b]

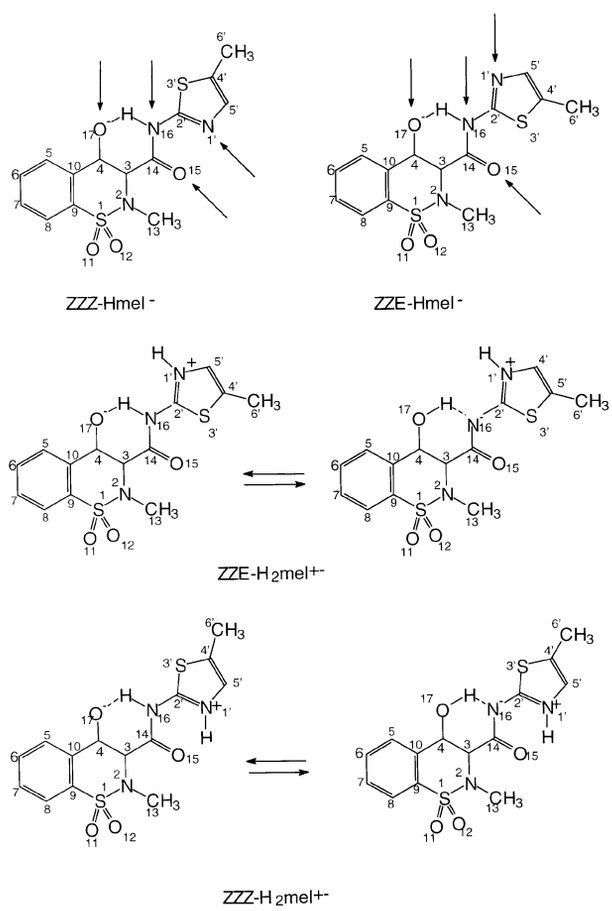

Scheme 2 Selected conformations for $Hmel^-$ and H_2mel^{+-}.

Density functional methods. All the density functional calculations were carried out using the GAUSSIAN 98 package[29]

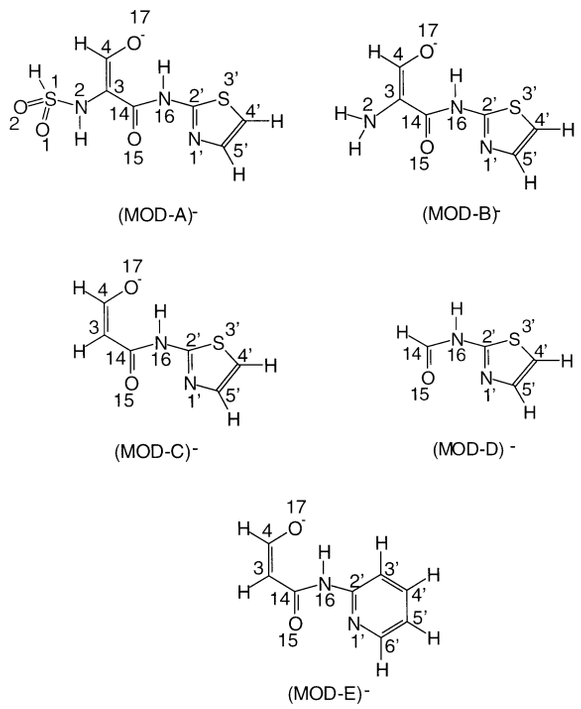

Scheme 3 The structural formulae used to model the $Hmel^-$ and $Hpir^-$ anions through the quantum mechanics semi-empirical, and density functional computations.

implemented on an Origin 3800 SG machine at CINECA (Inter-University Computing Centre, Casalecchio di Reno, Bologna, Italy). Geometry optimisations, population analyses and vibrational frequency calculations were obtained by using the Becke3LYP method[30] and different basis sets[30] depending on the atom type and on the molecule. The models analysed were: *EZE*-H_2mel (Lanl2dz; 6-31G**, S), $(MOD\text{-}A)^-$ (Scheme 3) (6-31G**, all the atoms), $(MOD\text{-}B)^-$ (Lanl2dz; 6-31G**, S), $(MOD\text{-}C)^-$ (Lanl2dz; 6-31G**, S), $Zn(MOD\text{-}C)^+$ (Lanl2dz), $Zn(MOD\text{-}C)^+$ (Lanl2dz; 6-31G**, S), $Zn(MOD\text{-}C)_2$ (Lanl2dz), $Zn(MOD\text{-}C)_2$, $Cd(MOD\text{-}C)_2$, $Co(MOD\text{-}C)_2$ (quartet) and $Cu(MOD\text{-}C)_2$ (doublet) (Lanl2dz; 6-31G**). The Zn atom was set in the plane of the ligand for $Zn(MOD\text{-}C)^+$, whereas a planar-*trans* arrangement was imposed for the co-ordination sphere atoms of $Zn(MOD\text{-}C)_2$, $Cd(MOD\text{-}C)_2$ and $Co(MOD\text{-}C)_2$. The $Cu(MOD\text{-}C)_2$ model was not restrained to planarity. The structure optimisations were carried out according to the criteria implemented in the program. The analysis of the vibrational frequencies was carried out for *EZE*-H_2mel, $(MOD\text{-}A)^-$ (6-31G**), $(MOD\text{-}C)^-$ and $Zn(MOD\text{-}C)_2$ (Lanl2dz; 6-31G**, S), only. An imaginary frequency was computed for $Zn(MOD\text{-}C)_2$. Molecular drawings were obtained through the ORTEP-3[22] package.

Results and discussion

X-Ray structure of $[M^{II}(Hmel)_2(O\text{-dmso})_2]$ (M = Co, 1; Zn, 3; Cd, 4)

The complex molecules **1**, **3** and **4** are isostructural (Figs. 1–3 and Tables 2 and 3). The co-ordination spheres are pseudo-octahedral and the metal ions sit on the inversion centres. The $Hmel^-$ anions act as chelators through the N(1′) nitrogen atoms of the thiazole moieties and through the O(15) amidic oxygen atoms at the equatorial positions (with a *trans* arrangement). The apical co-ordination sites are occupied by the O(1D) oxygen atoms of the two dmso ligands. The octahedra are elongated at the apical positions, the effect being the largest for **3**. The M–N(1′) bond distances are 2.088(3), 2.060(4) and 2.254(2) Å, whereas the M–O(15) bond lengths are 2.083(4), 2.081(4) and 2.269(2) Å, for **1**, **3** and **4**, respectively. These

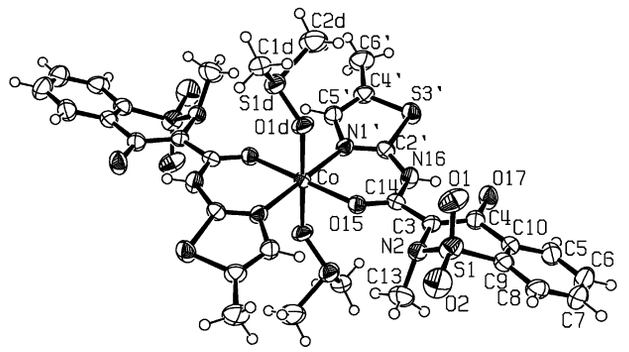

Fig. 1 Drawing of the complex molecule for $[Co^{II}(Hmel)_2(O\text{-dmso})_2]$, **1**. Ellipsoids enclose 30% probability. The labelling is reported for the atoms of the asymmetric unit, only.

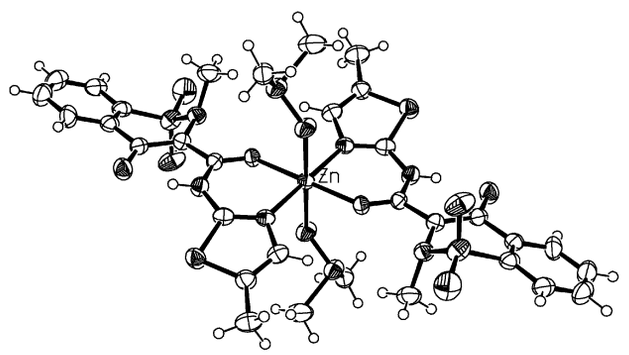

Fig. 2 Drawing of the complex molecule for $[Zn^{II}(Hmel)_2(O\text{-dmso})_2]$, **3**. Ellipsoids enclose 30% probability. The labelling of the ligand atoms is the same as for **1**.

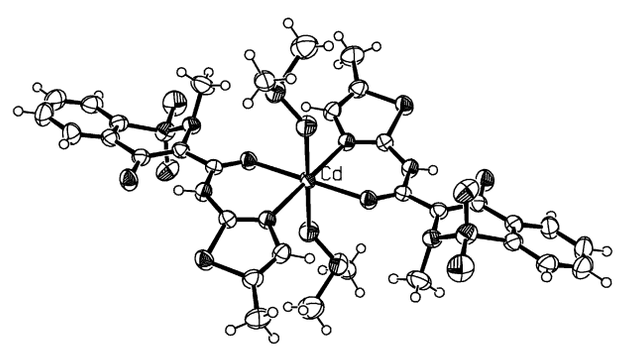

Fig. 3 Drawing of the complex molecule for $[Cd^{II}(Hmel)_2(O\text{-dmso})_2]$, **4**. Ellipsoids enclose 30% probability. The labelling of the ligand atoms is the same as for **1** and **3**.

experimental values show a good agreement with those predicted from the sum of the metallic radii and the covalent radii,[31] for **3** and **4** (differences smaller than 0.05 Å). The structure of **1** does not respect this trend, the predicted values being much smaller (up to 0.14 Å) than the experimental ones. The equatorial bond distances found for **4** agree well with the values previously found for the octahedral $[Cd^{II}(Hpir)_2(dmf)_2]$ (dmf = *N*,*N*-dimethylformamide) complex.[8a] The analysis of the puckering for the co-ordination ring of **1** on the basis of the Cremer and Pople model[32] gives a boat conformation (θ = 90(1)°) with a light screw component (ϕ = 25(1)°). The magnitude of the puckering is small, Q_T = 0.154(3) Å (Q_T = 0.630 Å for pure chair cyclohexane), and the N(16) and Co atoms deviate towards the same side by 0.120(4) Å from the plane defined by N(1′), C(2′), C(14) and O(15). Things are almost the same for **3** and **4**, except that the cadmium derivative has a significantly larger overall puckering (Q_T = 0.192(2) Å) and a smaller screw component (ϕ = 17.5(6)°).

Table 2 Selected bond lengths [Å] for $[Co(Hmel)_2(O\text{-dmso})_2]$, **1**, $[Zn(Hmel)_2(O\text{-dmso})_2]$, **3**, and $[Cd(Hmel)_2(O\text{-dmso})_2]$, **4**

Vector	Length		
	1	**3**	**4**
M–O(15)	2.083(3)	2.081(4)	2.2686(17)
M–N(1′)	2.088(3)	2.060(4)	2.254(2)
M–O(1D)	2.130(3)	2.173(4)	2.3133(18)
O(15)–C(14)	1.248(4)	1.235(6)	1.244(3)
N(1′)–C(2′)	1.303(5)	1.297(7)	1.297(3)
N(1′)–C(5′)	1.384(5)	1.388(7)	1.388(3)
N(16)–C(14)	1.368(5)	1.371(7)	1.383(3)
N(16)–C(2′)	1.371(5)	1.380(7)	1.371(3)
C(14)–C(3)	1.440(5)	1.443(7)	1.431(3)
C(3)–C(4)	1.394(6)	1.394(8)	1.399(3)
C(3)–N(2)	1.438(5)	1.436(7)	1.448(3)
S(3′)–C(4′)	1.729(4)	1.728(6)	1.733(3)
S(3′)–C(2′)	1.733(4)	1.733(6)	1.732(2)
S(1)–O(2)	1.423(3)	1.416(5)	1.431(2)
S(1)–O(1)	1.433(3)	1.431(5)	1.431(2)
S(1)–N(2)	1.633(4)	1.628(5)	1.625(2)
S(1)–C(9)	1.749(5)	1.740(6)	1.750(3)
O(17)–C(4)	1.263(5)	1.267(6)	1.272(3)
N(2)–C(13)	1.471(6)	1.476(7)	1.470(3)
C(5′)–C(4′)	1.337(6)	1.335(8)	1.336(4)
C(4′)–C(6′)	1.502(6)	1.496(8)	1.499(4)
C(4)–C(10)	1.506(6)	1.501(8)	1.498(3)
C(10)–C(9)	1.387(6)	1.392(8)	1.400(4)

Table 3 Selected bond angles [°] for $[Co(Hmel)_2(O\text{-dmso})_2]$, **1**, $[Zn(Hmel)_2(O\text{-dmso})_2]$, **3**, and $[Cd(Hmel)_2(O\text{-dmso})_2]$, **4**

Vector	Angle		
	1	**3**	**4**
O(15)–M–N(1′)#1	92.86(11)	92.65(16)	98.57(7)
O(15)–M–N(1′)	87.14(11)	87.35(16)	81.43(7)
O(15)–M–O(1D)	88.76(11)	88.97(15)	89.93(7)
O(15)#1–M–O(1D)	91.24(11)	91.03(15)	90.07(7)
N(1′)#1–M–O(1D)	91.56(13)	91.82(17)	93.79(8)
N(1′)–M–O(1D)	88.44(13)	88.18(17)	86.21(8)
C(14)–O(15)–M	129.6(2)	129.4(3)	130.60(15)
C(2′)–N(1′)–M	123.7(3)	124.2(4)	125.64(16)
C(5′)–N(1′)–M	124.7(3)	125.3(4)	122.81(16)
O(2)–S(1)–O(1)	118.9(2)	118.5(3)	118.95(15)
O(2)–S(1)–N(2)	108.6(2)	108.9(3)	108.52(13)
O(1)–S(1)–N(2)	108.59(19)	108.2(3)	108.53(11)
O(2)–S(1)–C(9)	110.3(2)	110.6(3)	109.81(14)
O(1)–S(1)–C(9)	107.6(2)	107.6(3)	107.99(13)
N(2)–S(1)–C(9)	101.5(2)	101.7(3)	101.64(12)
C(4′)–S(3′)–C(2′)	89.7(2)	89.5(3)	89.92(12)
C(2′)–N(1′)–C(5′)	110.6(3)	109.6(5)	110.9(2)
C(14)–N(16)–C(2′)	127.2(3)	126.1(5)	127.9(2)
O(15)–C(14)–N(16)	123.2(4)	123.6(5)	123.7(2)
O(15)–C(14)–C(3)	122.5(3)	123.0(5)	122.5(2)
N(16)–C(14)–C(3)	114.3(3)	113.5(4)	113.8(2)
C(4)–C(3)–N(2)	121.8(3)	121.1(5)	120.7(2)
C(4)–C(3)–C(14)	123.6(4)	124.3(5)	124.9(2)
N(2)–C(3)–C(14)	114.6(3)	114.6(5)	114.4(2)
O(17)–C(4)–C(3)	124.6(4)	124.1(5)	123.7(2)
O(17)–C(4)–C(10)	117.3(4)	117.1(5)	117.0(2)
C(3)–C(4)–C(10)	118.1(4)	118.8(5)	119.2(2)
C(3)–N(2)–C(13)	116.0(4)	115.9(5)	116.0(2)
C(3)–N(2)–S(1)	113.8(3)	114.0(4)	114.03(16)
C(13)–N(2)–S(1)	116.1(3)	116.3(4)	117.26(18)
C(4′)–C(5′)–N(1′)	116.5(4)	117.4(5)	116.6(2)
N(1′)–C(2′)–N(16)	127.1(4)	126.9(5)	127.8(2)
N(1′)–C(2′)–S(3′)	113.9(3)	114.7(4)	113.77(18)
N(16)–C(2′)–S(3′)	119.0(3)	118.3(4)	118.41(18)
C(5′)–C(4′)–C(6′)	129.5(4)	129.8(6)	129.6(3)
C(5′)–C(4′)–S(3′)	109.2(3)	108.8(4)	108.86(19)
C(6′)–C(4′)–S(3′)	121.3(3)	121.3(5)	121.5(2)

The $Hmel^-$ ligand

The meloxicam ligand is deprotonated at O(17) and adopts the 17,1′-*ZZZ* conformation. The chelating anion is stabilised by a strong intramolecular hydrogen bond which involves the O(17) and the N(16) atom (O ··· N, 2.558(3) Å; O ··· H–N, 137.9(5)° for **4**). The thiazole system maintains the coplanarity upon metal co-ordination and the corresponding bond distances are equal within two times the e.s.d.s to those for free H_2mel.[33] The C(3)–C(4) bond distance is 1.394(6), 1.394(8) and 1.399(3) Å for **1**, **3** and **4**, respectively, slightly longer than the corresponding value for metal-free and fully protonated H_2mel (1.363(3) Å).[33] In contrast the O(17)–C(4) bond distance is 1.263(5), 1.267(6) and 1.272(3) Å, for **1**, **3** and **4**, shorter than the value found for H_2mel (1.336(2) Å).[33] These values can be explained through the deprotonation at O(17) and agree with a significant π conjugation in the system O(17)/N(1′). The bond angle O(17)–C(4)–C(3) is in the range 123.7(2)–124.6(4)° and does not change much with respect to H_2mel and $NH_4^+Hmel^-$ (123.2(2) and 124.1(2)°).[33] In contrast the bond angles around C(3), C(14), N(16), C(2′) change significantly on passing from free H_2mel to **1**, **3** and **4** and $NH_4^+Hmel^-$. For instance, the C(4)–C(3)–C(14) angle is 124.9(2)° for **4** and 124.8(2)° for $NH_4^+Hmel^-$, and 120.9(2)° for H_2mel;[33a] the differences are even larger for N(16)–C(2′)–N(1′) which is 127.8(2)° for **4**, and 120.7(2)° for H_2mel and 121.1(2)° $NH_4^+Hmel^-$.[33a] The N(16)–C(2′)–N(1′) bond angles are smaller for the $Hpir^-$ (Cd, 122.4(4)°[8a]) than for the $Hmel^-$ derivatives; whereas the angles at N(16) are smaller (by *ca.* 5°) for the $Hmel^-$ (126.1–127.9°) derivatives when compared to the $Hpir^-$ ones. The O(17)–C(4)–C(3)–C(14)(O(15))–N(16)–C(2′) system is almost coplanar for free H_2mel (largest deviation from the least-squares plane, C(14), 0.069(4) Å; torsion around N(16)–C(14), 178.8(2)°) but is more distorted for the complexes (largest deviation, N(16) of **4**, 0.111(3) Å; torsion around N(16)–C(14), 166.3(2)°). The thiazine ring has an envelope conformation (with a small screw character), the N(2) atom being out of the plane defined by C(3), C(4), C(5), C(10) and S(1). The puckering parameters[32] for **4** are, $\theta = 65.1(3)°$, $\phi = 22.3(3)°$, and $Q_T = 0.552(2)$ Å. It has to be noted that the conformation for free H_2mel is a screw half-chair.[33a] This means that the thiazine moiety of the oxicam class of drugs is flexible at least upon deprotonation at O(17) and metal co-ordination at O(15) and N(1′).

Dmso ligand

The ambidentate dmso ligand co-ordinates the metal centre through the oxygen atom (O(1D)) for **1**, **3** and **4**. The preference for the *O*-dmso co-ordination mode over the *S*-dmso one can be explained by the relatively hard character of the cations used in this work (especially for Co(II) and Zn(II)) and on the basis of steric reasons. The O(1D)–S(1D) bond distance ranges 1.512(4)–1.521(3) Å for the three complexes, whereas it is 1.46(1) Å (average) for *trans*-$[PtCl_2(N1'\text{-}H_2pir)(S\text{-dmso})]$.[8b] The O–S(1D)–C bond angles are in the range 104.5(2)–105.3(3)°.

Crystal packing

Intermolecular stacking interactions exist between the thiazole moiety and the O(17)–C(4)–C(3)–C(14) system as is revealed by the overlap between the atoms and the contact distances (shortest contact: C(2′a) ··· O(17b) $(-x, -y - 1, -z)$, 3.312(4) Å, **4**). Weak intermolecular H-bond type interactions occur between O(1) and H(2d/3)–C(2D) $(-x + 1, -y, -z)$ (O ··· C, 3.351(4) Å; O ··· H, 2.55 Å; O ··· H–C, 141(1)°, **4**), and between O(2) and H(6′)–C(6′) $(x, y, z + 1)$ (O ··· C, 3.132(4) Å; O ··· H, 2.58 Å; O ··· H–C, 117(1)°, **4**). Therefore the complex molecules have an overall hydrophobic character as regards the exterior surface.

Spectroscopy

^{1}H NMR. The analysis of the chemical shifts for the signals of **3** ($CDCl_3$, Table 4) shows that the peaks attributable to the benzene system C(5)H, C(6)H, C(7)H and C(8)H protons occur

Table 4 ^{1}H NMR chemical shifts (ppm) for **3** and H_2mel (0.01 mol dm^{-3}, $CDCl_3$, 298 ± 1 K, 600 MHz)

Proton	**3**	H_2mel
H(17)	—	12.72
H(16)	9.66	10.20
H(5)	8.14	8.07
H(8)	7.78	7.91
H(6)	7.69	7.76
H(7)	7.62	7.76
H(5′)	7.43	7.28
H(13)	2.95	2.85
H(dmso)	2.66	—
H(6′)	2.40	2.44

at 8.14 (doublet, 1H), 7.69 (triplet, 1H), 7.62 (triplet, 1H) and 7.78 ppm (doublet, 1H), respectively. The signal for the C(5)H proton undergoes a small downfield shift (0.07 ppm) upon complexation and deprotonation when compared to the spectrum of free H_2mel (see ref. 33*a* for the spectrum of H_2mel in dmso-d_6), whereas the signals for the C(6)H, C(7)H and C(8)H protons experience some upfield shifts. The signal relevant to the thiazole C(5′)H proton for **3** (7.43 ppm, singlet, 1H) is shifted downfield by 0.15 ppm when compared to that found for free H_2mel. It has to be noted that the largest effect upon complexation is experienced by the signal (broad peak) for the N(16)H proton which occurs at 9.66 (1H) and 10.20 ppm (1H) for **3** and H_2mel, respectively. This is in agreement with the metal co-ordination to two atoms (O(15) and N(1′)) which are close to the N(16)H function and with the strong O(17) ⋯ H–N(16) hydrogen bond for the chelating $Hmel^-$ anion (see above). No signal was observed in the region 9–15 ppm for the spectrum of **3**, whereas a broad peak at 12.72 ppm (1H), attributable to the O(17)H proton is present in the spectrum of H_2mel. The spectrum of **4** ($CDCl_3$) has very broad signals. It seems reasonable to assume that dissociation of this complex occurs to a significant extent.

IR. The solid state spectra of **1**–**4** in KBr or nujol matrix are very similar (almost superimposable) in agreement with the strict similarity of the crystal and molecular structures. The stretching motion for the N–H bond which gives a sharp band at 3289 cm^{-1} in the spectrum of free H_2mel (nujol) does not give any detectable absorption in the spectra of compounds **1**–**4**, in agreement with the formation of the O(17) ⋯ H–N(16) intramolecular hydrogen bond. The stretching vibration for the amide C=O function absorbs at 1618 cm^{-1} for free H_2mel and in the range 1602–1614 cm^{-1} for **1**–**4**. The vibrations for the $>SO_2$ function give bands at 1346 (asymmetric stretching) and 1162 cm^{-1} (symmetric) in the spectrum of free H_2mel and at *ca.* 1336 and 1170 cm^{-1} for the metal complexes. A few comments on the computed spectra are reported below.

Molecular modelling

Molecular mechanics. The computed values for the strain energies of the free H_2mel show that the *EZE*-conformation is preferred when compared to *EZZ* (by 27.070 kJ) and to *ZZZ* (by 31.322 kJ). The analysis agrees well with the *EZE*-conformation found *via* X-ray diffraction in the solid state.[33] The selected computed geometrical parameters for *EZE*-H_2mel and $Zn(Hmel)_2$, as well as the selected force field parameters are listed in Table 5. The computed bond distances are usually very close for the three conformations except for the C(3)–C(14) bond distance which is longer by 0.049 Å in the *EZE*-conformation with respect to *EZZ* and *ZZZ*. In contrast, the computed N(16)–C(2′) bond distance is shorter by 0.036 Å in the *EZE*-conformation. The computed bond angles for the three conformations do not differ more than 5° from the experimental values of the solid state structures. The computed structure for *trans*,*trans*-$Zn(Hmel)_2$ shows an acceptable agreement with the experimental structure of **3** (differences in bond lengths are smaller than 0.06 Å, Table 5). The analysis shows that the molecular mechanics method is a reliable and fast tool to study the conformational space of this type of molecule.

Semi-empirical methods. Structures. The geometry optimisations for all the molecules investigated (see above) *via* the ZINDO/1 method[27a,b] converged nicely. Other semi-empirical methods, namely MNDO, MNDO/d, INDO, CNDO, AM1 and PM3,[26b] failed to reproduce the available solid state structures at an acceptable degree of accuracy (at least with the default parameters implemented in HyperChem[26]). The computed bond distances for H_2mel are usually within 0.03 Å of the experimental values, except for the S(1)–O/N bonds; the computed S(1)–O length is larger, by 0.3 Å, than the experimental one, and the computed C(14)–O(5) bond distance is larger by *ca.* 0.08 Å than the found one. An acceptable agreement between computations and experiments was found for the $Hmel^-$ anion, the H_3mel^+ cation and the zwitterionic H_2mel^{+-}, too. Therefore, the semi-empirical method ZINDO/1 is a convenient modelling tool for this type of ligand (even though the S–O bond distances are not finely predicted and should be restrained). The computed structure of $(MOD\text{-}B)^-$ (Scheme 3) and even $(MOD\text{-}C)^-$ models reproduce well the relevant moieties of $Hmel^-$, whereas $(MOD\text{-}D)^-$ did not reproduce properly the amide moiety of the anionic form of the real ligand. As a consequence, $(MOD\text{-}C)^-$ and $(MOD\text{-}E)^-$ were adopted as the optimal models for $Hmel^-$ and $Hpir^-$. The optimised structures of $M(MOD\text{-}C)^+$ nicely reproduce the bond distances for the relevant ligand moieties found in the solid state for **1**, **3** and **4**. As expected the computed Zn–N/O lengths are shorter than those found in the solid state, owing to the small co-ordination number of the models. The trends for the computed M–donor bond distances for Zn- and Cd-$(MOD\text{-}C)^+$ are in good agreement with the observed ones. The computed Cu–N/O bond distances for $Cu(MOD\text{-}C)^+$ are smaller than the values relevant to the Zn(II)-model, in agreement with well documented experimental values (see for instance the M–N/O, M = Zn(II) and Cu(II), distances reported in refs.34*a*, *b*). The computed Zn–O and Zn–N bond distances for tetra-co-ordinate $Zn(MOD\text{-}C)_2$ are 2.011 and 1.962 Å, respectively, not very far from the values of 2.081(4) and 2.060(4) Å found for hexa-coordinate **3**. The computed O–C bonds are longer by 0.07 Å with respect to those found for **3**, all the other computed bond lengths are within 0.05 Å of the experimental values.

Energy. The computed heats of formation (ΔH_f^{298}) for the selected optimised structures are listed in Table 6. The most favourable conformations for H_2mel are of the *E* type at C(3)–C(14) and are stabilised by the O–H ⋯ O hydrogen bond. The *Z*-type structures at C(3)–C(14) would allow the formation of weaker HO ⋯ H–N interactions, and are less stable by *ca.* 92 kJ. The energy barrier for the rotation around C(3)–C(14) is *ca.* 243 kJ. As expected, the *Z*-$Hmel^-$ conformation at C(3)–C(14) is more favoured when compared to the *E* conformation (by 201 kJ) due to the stabilising effect of the $^-O(17)$ ⋯ H–N(16) hydrogen bond. The computed enthalpy barrier for rotation around C(3)–C(14) in $Hmel^-$ is *ca.* 373 kJ. This means that the rotations around C(3)–C(14) for *E*-H_2mel and *Z*-$Hmel^-$ are thermodynamically and kinetically unfavourable and must be thermally assisted and/or assisted by protonation/deprotonation (at O(17)) and metal complex formation/dissociation (at O(15)). The computed difference between the formation enthalpies for the *E* and *Z* conformations at N(16)–C(2′) is small (*ca.* 1–4 kJ) whereas the computed energy barrier for full rotation is *ca.* 21 kJ, a value which is compatible with the bond formation energies of several types of hydrogen bonds.[35] The favoured form for H_2mel in the gas phase is the zwitterionic one, H_2mel^{+-}, by 116 kJ. This is explained by the formation of two

Table 5 Selected geometrical parameters (lengths/Å; angles/°) for *EZE*-H_2mel and $Zn(Hmel)_2$ optimised *via* the molecular mechanics method and force field parameters used for the co-ordination sphere of $Zn(Hmel)_2$. The Van der Waals parameters used for Zn were: *r*, 2.00 Å; *ε*, 2.637 kJ

Vector	*EZE*-H_2mel Computed	*EZE*-H_2mel X-ray [33]	$Zn(Hmel)_2$ Computed	**3** X-ray
S(1)–N(2)	1.625	1.636(2)	1.623	1.628(5)
N(2)–C(3)	1.409	1.440(2)	1.410	1.436(7)
C(3)–C(4)	1.405	1.363(3)	1.425	1.394(8)
C(4)–O(17)	1.368	1.336(2)	1.225	1.267(7)
S(1)–O(1)	1.450	1.429(2)	1.451	1.431(5)
C(3)–C(14)	1.487	1.451(3)	1.494	1.443(7)
C(14)–O(15)	1.222	1.246(2)	1.231	1.235(6)
C(14)–N(16)	1.398	1.353(3)	1.341	1.371(7)
N(16)–C(2′)	1.399	1.391(2)	1.429	1.379(6)
C(2′)–S(3′)	1.735	1.727(2)	1.730	1.733(6)
C(2′)–N(1′)	1.287	1.293(2)	1.287	1.297(7)
C(3)–C(4)–O(17)	120.4	123.2(3)	121.1	124.1(5)
C(4)–C(3)–C(14)	120.9	120.8(5)	122.4	124.3(5)
C(3)–C(14)–O(15)	119.5	121.1(3)	117.6	123.0(5)
C(3)–C(14)–N(16)	118.6	117.6(5)	116.4	113.5(4)
C(14)–N(16)–C(2′)	127.0	124.5(2)	123.3	126.1(4)
N(16)–C(2′)–S(3′)	124.2	123.1(1)	117.9	118.3(4)
N(16)–C(2′)–N(1′)	118.3	120.7(2)	129.5	126.9(5)
O(17)–C(4)–C(3)–C(14)	5.4	0.6(3)	−4.3	−0.9(9)
N(2)–C(3)–C(14)–N(16)	−11.6	−5.8(2)	−179.9	−178.5(4)
C(3)–C(14)–N(16)–C(2′)	179.8	−178.1(2)	175.9	−168.5(5)
C(4)–C(3)–C(14)–N(16)	−7.1	−5.1(2)	1.4	1.7(8)
C(14)–N(16)–C(2′)–S(3′)	−0.4	−1.2(4)	176.2	159.4(4)

Vector	Force constant/kJ $Å^{-2}$ mol^{-1}	Equilibrium distance/Å
Zn–N	544.154	2.06
Zn–O	502.296	2.08

Vectors	Force constant/kJ rad^{-2} mol^{-1}	Equilibrium angle/°
O–Zn–O	125.574	180.0
N–Zn–N	125.574	180.0
O–Zn–N	62.787	90.0
Zn–O–C	104.645	120.0
Zn–N–C	104.645	120.0
Zn–N–C–X	V1, 0.0; V2, 41.858; V3, 0.0	
Zn–O–C–X	V1, 0.0; V2, 41.858; V3, 0.0	

strong hydrogen bonds, namely $^{-}O(17) \cdots H–N(16)$ and $O(15) \cdots H–N(1')^{+}$. Finally, the enthalpies for the complex formation of $M^{II}(MOD\text{-}C)^{+}$ are −2158, −3228, −3092, −2903 and −2711 kJ, for Cd(II), Zn(II), Cu(II) (doublet), Ni(II) (triplet) and Co(II) (quartet) derivatives respectively, whereas the value for the overall formation of $Zn(MOD\text{-}C)_2$ is −5001 kJ. The small heat of formation for $Cd(MOD\text{-}C)^{+}$ when compared to the other 1 : 1 metal chelates predicts an instability for **4** in solution (see above, NMR and UV experimental data). Finally, the heat of complex formation for $Zn(MOD\text{-}E)^{+}$ is −3285 kJ, showing that the $Hpir^{-}$ anion is more effective than $Hmel^{-}$ in chelating "block-d" divalent cations.

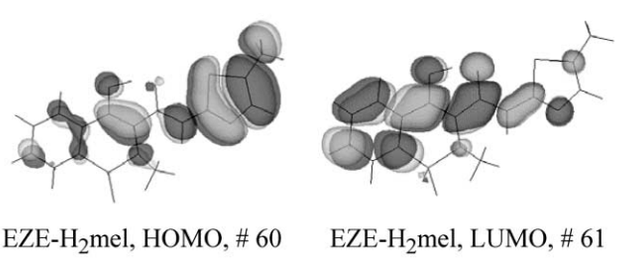

Fig. 4 Representation of the HOMO and LUMO for *EZE*-H_2mel as computed at the semi-empirical ZINDO/1–ZINDO/S level.

UV. The computed spectrum for *EZE*-H_2mel has a major peak at 364 nm (oscillator strength, 0.815) which compares well with the experimental absorption maximum at 343 nm (in $CHCl_3$). The peak is due to the HOMO–LUMO transition *i.e.* a charge transfer from thiazole to benzothiazine (Fig. 4). The π–π overlap weighting factor had to be changed from the default value (0.585) to 0.660 to match the experimental spectrum. A red shift is computed for the zwitterion, *ZZZ*-H_2mel^{+-}, 394 nm, and for the anion *ZZE*-$Hmel^{-}$, 372 nm. The computed spectrum for $(MOD\text{-}C)^{-}$ has an intense effect at 297 nm which is red shifted upon complexation; in fact, the spectrum for $Zn(MOD\text{-}C)^{+}$ has an intense peak at 333 nm due to the HOMO–LUMO + 1 transition, *i.e.* a ligand (mostly thiazole) to metal charge transfer transition. The computed intense band at 313 nm for $Zn(MOD\text{-}C)_2$ is attributable to the HOMO–LUMO + 1 and HOMO − 1–LUMO transitions which correspond to charge transfer from thiazole to the $^{-}O–CH{=}CH–C(=O)–$ function. It is reasonable to assume that the intense peak found in the real spectra of **1**–**3** at *ca.* 370 nm is due to a similar charge transfer from thiazole to the amide–benzothiazine region.

Density functional methods. Structures. With the aim to search for a fast modelling tool able to give an even better agreement between the computed and experimental structures, the calculations on selected molecules were extended to the density functional Becke3LYP method by using different basis

sets (see above; Molecular mechanics, Density functional methods). The *EZE*-H_2mel molecule (X-ray structure as the starting model) as well as the molecules $(MOD\text{-}A)^-$, $(MOD\text{-}B)^-$ and $(MOD\text{-}C)^-$ (Scheme 3), used as models for the *ZZZ*-$Hmel^-$ anion, were optimised. The analysis of the geometrical parameters (see Table 7 for the selected bond distances) for the computed *EZE*-H_2mel molecule shows a good agreement with the structure found in the solid state. In fact, the largest deviation is relevant to the C(5′)–C(4′) bond (0.054 Å) and most of the other bond distances have deviations smaller than 0.03 Å. The computed S–O bond distances are 1.469 Å and they compare well with the experimental values, 1.426 Å. As regards the simulations for the *ZZZ*-$Hmel^-$ ligand even

Table 6 Heats of formation and heats of reaction for selected molecules and reactions (ΔH_f^{298} and ΔH_r^{298}/kJ mol^{-1}, 298 K) as computed *via* the quantum mechanics semi-empirical method

Model	ΔH_f^{298}/kJ	Model	ΔH_f^{298}/kJ
EZZ-H_2mel	−29426.647	$Zn(MOD\text{-}C)^+$	−13322.133
EZE-H_2mel	−29425.730	$Zn(MOD\text{-}E)^+$	−16754.673
ZZZ-H_2mel	−29330.177	$Cd(MOD\text{-}C)^+$	−12410.981
ZZE-H_2mel	−29334.174	$Cu(MOD\text{-}C)^+$ doub.	−12961.300
ZZZ-H_2mel^{+-}	−29542.347	$Ni(MOD\text{-}C)^+$ trip.	−13164.709
EZZ-H_3mel^+	−29687.288	$Co(MOD\text{-}C)^+$ quart.	−13060.223
EZZ-$Hmel^-$	−28609.993	$Zn(MOD\text{-}C)_2$	−27923.631
ZZE-$Hmel^-$	−28809.907	Zn^{2+}	2733.809
ZZZ-$Hmel^-$	−28810.811	Cd^{2+}	2574.991
$(MOD\text{-}B)^-$	−13973.611	Cu^{2+} doub.	2958.821
$(MOD\text{-}C)^-$	−12827.983	Ni^{2+} trip.	2566.251
$(MOD\text{-}D)^-$	−9248.086	Co^{2+} quart.	2479.107
$(MOD\text{-}E)^-$	−16203.964	H^+	1478.755

Reaction	ΔH_r^{298}/kJ
EZZ-$Hmel^- + H^+ \longrightarrow$ *EZZ*-H_2mel	−2295.409
ZZZ-$Hmel^- + H^+ \longrightarrow$ *ZZZ*-H_2mel	−1998.121
ZZE-$Hmel^- + H^+ \longrightarrow$ *ZZE*-H_2mel	−2003.023
ZZZ-$Hmel \longrightarrow$ *ZZZ*-H_2mel^{+-}	−212.170
EZZ-$Hmel + H^+ \longrightarrow$ *EZZ*-H_3mel^+	−1739.397
$(MOD\text{-}C)^- + Zn^{2+} \longrightarrow Zn(MOD\text{-}C)^+$	−3227.959
$(MOD\text{-}E)^- + Zn^{2+} \longrightarrow Zn(MOD\text{-}E)^+$	−3284.608
$(MOD\text{-}C)^- + Cd^{2+} \longrightarrow Cd(MOD\text{-}C)^+$	−2157.989
$(MOD\text{-}C)^- + Cu^{2+}$ doub. $\longrightarrow Cu(MOD\text{-}C)^+$	−3092.138
$(MOD\text{-}C)^- + Ni^{2+}$ trip. $\longrightarrow Ni(MOD\text{-}C)^+$	−2902.978
$(MOD\text{-}C)^- + Co^{2+}$ quart. $\longrightarrow Co(MOD\text{-}C)^+$	−2711.348
$2(MOD\text{-}C)^- + Zn^{2+} \longrightarrow Zn(MOD\text{-}C)_2$	−5001.474

$(MOD\text{-}C)^-$, as optimised by using the (Lanl2dz; 6-31G**, S) basis set, has a good agreement with the relevant moiety of the $Hmel^-NH_4^+$ salt,[33a] the largest difference for the bond distances being that relevant to S(3′)–C(2′) (0.057 Å, computed is larger than found). The presence of the NH_2 group on the C(3) atom, $(MOD\text{-}B)^-$, or that of the HN–SO_2H group, $(MOD\text{-}A)^-$, does not change much the bond distances when compared to $(MOD\text{-}C)^-$. The optimised structure of $Zn(MOD\text{-}C)_2$ at the Becke3LYP/(Lanl2dz; 6-31G**, S) (Fig. 5, Table 7) level has

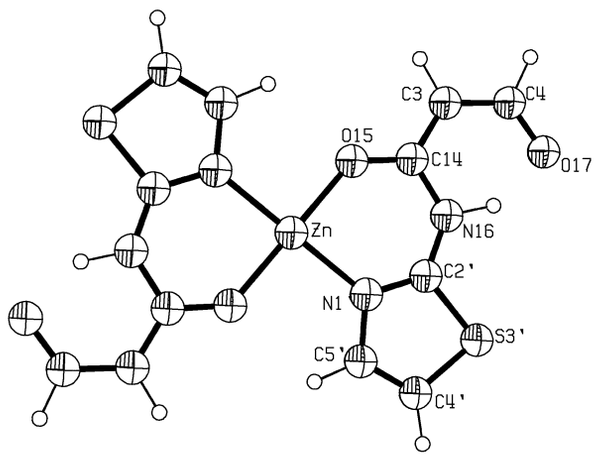

Fig. 5 ORTEP type representation for $Zn(MOD\text{-}C)_2$ as optimised at the density functional Becke3LYP/(Lanl2dz; 6-31G**, S) level.

Zn–O(15) and Zn–N(1′) bond distances of 1.997 and 2.065 Å, which compare well with the values found for **3**. As expected, the S–C bond distances (thiazole) are significantly improved by the use of the more accurate 6-31G** basis set for sulfur atoms and are C(2′)–S(3′), 1.759; S(3′)–C(4′), 1.748 Å, for the bis-chelate in almost perfect agreement with **3**. Analogous to the $Zn(MOD\text{-}C)_2$ model, the Co, Cu and Cd counterparts have good theory (Table 7)–experiment agreement.

Vibrational frequencies. Selected normal frequencies and IR intensities as computed for *EZE*-H_2mel, $(MOD\text{-}A)^-$ and $Zn(MOD\text{-}C)_2$ are compared with the experimental values for the free H_2mel ligand and the complex molecules **1**–**4** in Table 8. The experimental and computed values show an overall good agreement. However, the N–H stretching vibration for H_2mel

Table 7 Selected bond distances (Å) for some of the molecules optimised *via* the density functional Becke3LYP method. Experimental values for *EZE*-H_2mel, $Hmel^-$ and **3** are also reported for comparison purposes

	Distance								
	Computed								
			$M(MOD\text{-}C)_2$				Found		
Vector	*EZE* H_2mel	$(MOD\text{-}C)^-$	Co	Cu	Zn	Cd	*EZE* H_2mel (ref. 33)	$Hmel^-$ (ref. 33)	**3**
N(2)–C(3)	1.445						1.437	1.449	1.436
O(17)–C(4)	1.364	1.303	1.293	1.294	1.294	1.295	1.330	1.285	1.267
C(4)–C(3)	1.386	1.410	1.426	1.425	1.425	1.423	1.366	1.384	1.394
C(3)–C(14)	1.461	1.436	1.407	1.409	1.409	1.411	1.461	1.445	1.443
C(14)–O(15)	1.288	1.286	1.316	1.316	1.312	1.310	1.238	1.244	1.235
C(14)–N(16)	1.369	1.417	1.410	1.405	1.413	1.418	1.357	1.366	1.371
N(16)–C(2′)	1.401	1.372	1.363	1.363	1.364	1.365	1.401	1.382	1.380
C(2′)–N(1′)	1.326	1.340	1.351	1.348	1.351	1.351	1.298	1.305	1.297
N(1′)–C(5′)	1.394	1.394	1.404	1.403	1.404	1.404	1.388	1.385	1.388
C(5′)–C(4′)	1.382	1.379	1.368	1.368	1.369	1.369	1.328	1.341	1.335
C(4′)–S(3′)	1.756	1.756	1.749	1.748	1.748	1.747	1.729	1.732	1.728
S(3′)–C(2′)	1.757	1.780	1.757	1.755	1.759	1.764	1.721	1.723	1.733
S(1)–N(2)	1.684						1.642	1.632	
S(1)–O(1)	1.469						1.426	1.434	
M–O(15)			1.984	1.956	1.997	2.172			2.081
M–N(1′)			2.033	1.985	2.065	2.242			2.060

Table 8 Selected normal vibrations (ν, stretching; δ, bending) in cm^{-1}. The intensities are: w, weak; m, medium; s, strong; sh, shoulder, with the values in parentheses in km mol^{-1}. The diagonal elements of the force constant matrix are in square brackets in mdyne $Å^{-1}$ or in mdyne rad^{-1}. Selected experimental data for some compounds are reported for comparative purposes

Species	$\nu_{sym}SO_2$	$\delta + \nu$ thiazole	$\nu_{asym}SO_2$	$\nu + \delta$ thiazole	νCO + δ NH amide	NH amide
Computed						
EZE-H_2mel	1115 w(54.7) [3.372]	1164 w(73.6) [1.974] 1176 w(23.4) [2.048]	1317 m(153.3) [10.061]	1566 w(5.6) [5.708] 1538 w(13.1) [6.608]	1608 w(16.4) [5.707] 1593 w(54.7) [9.085] 1571 s(1117.4) [5.015]	3586 w(70.3) [8.161]
$(MOD\text{-}A)^-$	1125 m(156.7) [2.654]	1161 s(196.2) [1.752]	1317 m(168.8) [4.876]		1591 s(1332.7) [4.201]	
$Zn(MOD\text{-}C)_2$		1180 m(132.4) [1.820]		1559 s(507.7) [11.096]	1585 s(253.8) [5.591]	
Found (nujol)						
EZE-H_2mel	1162 m	1184 m	1345 s	1586 sh	1618 m 1549 s 1530 s	3289 s
1	1168 m	1186 w	1335 s	1558 w	1603 s 1572 sh	
2	1167 m	1185 m	1336 s	1558 w	1602 s 1577 sh	
3	1171 m	1186 m	1335 s	1557 w	1605 s 1570 sh	
4	1171 m	1188 m	1337 s		1614 s 1570 sh	

was computed at 3586 cm^{-1}, whereas the relevant absorption band in the real spectrum of *EZE*-H_2mel is at 3289 cm^{-1}. This significant difference can have a rationale in the intermolecular N–H ··· $O(SO_2)$ hydrogen bond (d(N ··· O), 3.028 Å) which takes place in the solid state.[33] The computed frequencies for the almost pure asymmetric and symmetric stretching vibrations for the $>SO_2$ group of H_2mel (gas phase) are 1317 and 1115 cm^{-1}, respectively, whereas the absorption bands in the real spectrum of crystalline H_2mel, which can be reasonably associated to these motions, occur at 1345 and 1162 cm^{-1}. The computed frequencies mainly associated with the O=C–N–H amide group are 1608, 1593, and 1571 cm^{-1}, which can be related to the bands at 1618, 1549, and 1530 cm^{-1} in the spectrum of crystalline H_2mel. The computed frequencies at 1559 and 1180 cm^{-1} due to the combined movements for the thiazole ring atoms (especially C(2′), S(3′) and C(4′)) for $Zn(MOD\text{-}C)_2$ can be related to the experimental values at *ca.* 1557 and 1186 cm^{-1} for **1**–**3**.

Conclusion

This work details the synthesis and the structural characterisation of the first series of metal complexes with the widely used anti-inflammatory drug meloxicam (mono-anionic form). The Co(II) and Zn(II) derivatives are themselves potential anti-inflammatory drugs. All the four complexes (M = Co **1**, Ni **2**, Zn **3** and Cd **4**) were obtained at high yield through simple reaction of the relevant metal acetate and the drug in alcohol and dmso. The meloxicam molecule acts as a mono-anionic chelating ligand through the amide oxygen and the thiazolyl nitrogen. Therefore the change of thiazolyl (meloxicam) for pyridyl (piroxicam) does not alter the co-ordination mode of this class of ligand and the enolate oxygen atom is still not active as a donor, at least for Co(II), Zn(II) and Cd(II). The complexes **1**, **3** and **4** have no strong intermolecular contacts in the unit cell and have no co-crystallised water molecules even though the crystal growth procedures were carried out in air. This confirms the hydrophobic character of the complex molecules which is important for the potential pharmacological properties. The hydrophobicity of metal based pharmaceuticals is desired to help prevent their decomposition in biological buffer solutions and is believed to facilitate their transport through the cell membranes.[3e] Furthermore, the formation of stable bis-chelates protects the drug molecules from enzymatic degradation. The atomic charges for the external atoms O(17), H(16) and S(3′) (as computed for $Zn(MOD\text{-}C)_2$, a reliable model for $Zn(Hmel)_2$, through the Mulliken population analysis based on density functional theory) have a root mean square deviation from zero (0.386 e) unchanged with respect to $(MOD\text{-}C)^-$ (0.387 e); in addition, the highly negative O(15) and N(1′) atoms of free $Hmel^-$ are linked to the di-positive metal ion and are hidden in the internal part of the bis-chelates. The view of the electrostatic potential surfaces for selected model systems, as obtained through HyperChem-ZINDO/1, helps to evaluate the hydrophobicity of the $Zn(Hmel)_2$ chelate (see ESI†). Finally, this work compares the usage of various molecular modelling tools, a comparison which may help in the selection of computational strategies for this type of molecule in future investigations. The combined semi-empirical ZINDO/1 and ZINDO/S methods are appropriate for geometrical optimisations and for predicting reliable UV spectra and formation enthalpies. The density functional procedures at the Becke3LYP/(Lanl2dz; 6-31-G**, S) level allow the computations of high quality structures, reliable IR spectra and atomic charges.

Acknowledgements

The authors gratefully thank Boehringer-Ingelheim Italia (Reggello, Florence) for a generous gift of meloxicam. The authors thank also Mr Francesco Berrettini for the X-ray data collection at Centro Interdipartimentale di Analisi e Determinazioni Strutturali (CIADS), University of Siena. Ministero della Università e della Ricerca Scientifica e Tecnologica (MURST), Consiglio Nazionale delle Ricerche (CNR) and the University of Siena, are acknowledged for funding.

References

1 (*a*) C. Orvig and M. J. Abrams, *Chem. Rev.*, 1999, **99**, 2201; (*b*) K. H. Thompson, J. H. McNeill and C. Orvig, *Chem. Rev.*, 1999, **99**, 2561; (*c*) H. Sun, H. Li and P. J. Sadler, *Chem. Rev.*, 1999, **99**, 2817.

2 *Uses of Inorganic Chemistry in Medicine*, ed. N. P. Farrell, Royal Society of Chemistry, Cambridge, UK, 1999, ch. 3; and references therein.

3 (*a*) J. E. Weder, T. W. Hambley, B. J. Kennedy, P. A. Lay, G. J. Foran and A. M. Rich, *Inorg. Chem.*, 2001, **40**, 1295; (*b*) Q. Zhou, T. W. Hambley, B. J. Kennedy, P. A. Lay, P. Turner, B. Warwick, J. R. Biffin and H. L. Regtop, *Inorg. Chem.*, 2000, **39**, 3742; (*c*) J. E. Weder, T. W. Hambley, B. J. Kennedy, P. A. Lay, D. MacLachlan, R. Bramley, C. D. Delfs, K. S. Murray, B. Moubaraki, B. Warwick, J. R. Biffin and H. L. Regtop, *Inorg. Chem.*, 1999, **38**, 1736.

4 Z. Guo and P. J. Sadler, *Angew. Chem., Int. Ed.*, 1999, **38**, 1512.

5 J. R. J. Sorenson, *Prog. Med. Chem.*, 1989, **26**, 437.

6 (*a*) S. K. Hadjikakou, M. A. Demertzis, J. R. Miller and D. Kovala-Demertzi, *J. Chem. Soc., Dalton Trans.*, 1999, 663; (*b*) D. M. Kovala-Demertzi, A. Theodorou, M. A. Demertzis, C. P. Raptopoulou and A. Terzis, *J. Inorg. Biochem.*, 1997, **65**, 151; (*c*) D. Kovala-Demertzi, D. Mentzafos and A. Terzis, *Polyhedron*, 1993, **12**, 1361.

7 C. Castellari, G. Feroci and S. Ottani, *Acta Crystallogr., Sect. C*, 1999, **55**, 907.

8 (*a*) R. Cini, G. Giorgi, A. Cinquantini, C. Rossi and M. Sabat, *Inorg. Chem.*, 1990, **29**, 5197; (*b*) R. Cini, *J. Chem. Soc., Dalton Trans.*, 1996, 111; (*c*) D. Di Leo, F. Berrettini and R. Cini, *J. Chem. Soc., Dalton Trans.*, 1998, 1993.

9 (*a*) R. Cini, *Comments Inorg. Chem.*, 2000, **22**, 151; (*b*) R. Cini, R. Pogni, R. Basosi, A. Donati, C. Rossi, L. Sabadini, L. Rollo, S. Lorenzini, R. Gelli and R. Marcolongo, *Met. Based Drugs*, 1995, **2**, 43.

10 M. S. Lüth, E. Freisinger and B. Lippert, *Chem. Eur. J.*, 2001, **7**, 2104.

11 L. G. Marzilli, S. O. Ano, F. P. Intini and G. Natile, *J. Am. Chem. Soc.*, 1999, **121**, 9133.

12 (*a*) U. Bierbach, M. Sabat and N. Farrell, *Inorg. Chem.*, 2000, **39**, 2960; (*b*) U. Bierbach, M. Sabat and N. Farrell, *Inorg. Chem.*, 2000, **39**, 3734.

13 (*a*) B. A. J. Jansen, J. van der Zwan, H. den Dulk, J. Brouwer and J. Reedijk, *J. Med. Chem.*, 2001, **44**, 245; (*b*) A. C. G. Hotze, A. H. Velders, F. Ugozzoli, M. Biagini-Cingi, A. M. Manotti-Lanfredi, J. G. Haasnoot and J. Reedijk, *Inorg. Chem.*, 2000, **39**, 3838.

14 R. Cini, M. Corsini and A. Cavaglioni, *Inorg. Chem.*, 2000, **39**, 5874.

15 (*a*) G. A. Higgs, E. A. Higgs and S. Moncada, in *Comprehensive Medicinal Chemistry*, ed. C. Hansch, P. G. Sammes, J. B. Taylor, J. C. Emmet, P. D. Kennewell and C. A. Ramsden, Pergamon Press, Oxford, 1990, ch. 6.2; (*b*) A. S. Kalgutkar, B. C. Crews and L. J. Marnett, *Biochemistry*, 1996, **35**, 9076; (*c*) E. S. Lazer, C. K. Miao, C. L. Cywin, R. Sorcek, H.-C. Wong, Z. Meng, I. Potocki, M.-A. Hoermann, R. J. Snow, M. A. Tschantz, T. A. Kelly, D. W. McNeil, S. J. Coutts, L. Churchill, A. J. Graham, E. David, P. M. Grob, W. Engel, H. Meier and G. Trummlitz, *J. Med. Chem.*, 1997, **40**, 980.

16 *Molecular Orbital Calculations for Biological Systems*, ed. A.-M. Sapse, Oxford University Press, Oxford, 1998.

17 P. Comba and T. W. Hambley, *Molecular Modeling of Inorganic Compounds*, Wiley-VCH, New York, 2nd edn., 2001.

18 XSCANS Users Manual, Siemens Analytical X-ray Instruments Inc., Madison, Wisconsin, USA, 1994.

19 XEMP, Empirical Absorption Correction Program, Siemens Analytical X-ray Instruments Inc., Madison, Wisconsin, USA, 1994.

20 G. M. Sheldrick, SHELXL-97, Program for the Refinement of Crystal Structures, University of Göttingen, 1997.

21 M. Nardelli, PARST-97, A System of Computer Routines for Calculating Molecular Parameters from Results of Crystal Structure Analyses, University of Parma, 1997.

22 C. K. Johnson and M. N. Burnett, ORTEP-3 for Windows, Oak Ridge National Laboratory, 32-bit Implementation by L. J. Farrugia, University of Glasgow, 1998.

23 L. Zsolnai, XPMA-ZORTEP-98, University of Heidelberg, 1998.

24 MacroModel, Interactive Molecular Modeling System, version 5.0, Department of Chemistry, Columbia University, 1995.

25 W. D. Cornell, P. Cieplak, C. I. Bayly, I. R. Gould, K. M. Merz, Jr., D. M. Ferguson, D. C. Spellmeyer, T. Fox, J. W. Caldwell and P. A. Kollman, *J. Am. Chem. Soc.*, 1995, **117**, 5179.

26 (*a*) HyperChem™, Molecular Modeling System, Release 5.1 Pro for Windows, Hypercube Inc., Gainesville, FL, 1997; (*b*) HyperChem™, *Reference Manual*, Hypercube Inc., Gainesville, FL, 1997.

27 (*a*) A. D. Bacon and M. C. Zerner, *Theor. Chim. Acta*, 1979, **53**, 21; (*b*) W. P. Anderson, W. D. Edwards and M. C. Zerner, *Inorg. Chem.*, 1986, **25**, 2728.

28 (*a*) J. E. Ridley and M. C. Zerner, *Theor. Chim. Acta*, 1976, **42**, 223; (*b*) J. Del Bene and H. H. Jaffe, *J. Chem. Phys.*, 1968, **48**, 1807. See also ref. 26*b*.

29 M. J. Frisch, G. W. Trucks, H. B. Schlegel, G. E. Scuseria, M. A. Robb, J. R. Cheeseman, V. G. Zakrzewski, J. A. Montgomery Jr., R. E. Stratmann, J. C. Burant, S. Dapprich, J. M. Millam, A. D. Daniels, K. N. Kudin, M. C. Strain, O. Farkas, J. Tomasi, V. Barone, M. Cossi, R. Cammi, B. Mennucci, C. Pomelli, C. Adamo, S. Clifford, J. Ochterski, G. A. Petersson, P. Y. Ayala, Q. Cui, K. Morokuma, D. K. Malick, A. D. Rabuck, K. Raghavachari, J. B. Foresman, J. Cioslowski, J. V. Ortiz, A. G. Baboul, B. B. Stefanov, G. Liu, A. Liashenko, P. Piskorz, I. Komaromi, R. Gomperts, R. L. Martin, D. J. Fox, T. Keith, M. A. Al-Laham, C. Y. Peng, A. Nanayakkara, M. Challacombe, P. M. W. Gill, B. Johnson, W. Chen, M. W. Wong, J. L. Andres, C. Gonzalez, M. Head-Gordon, E. S. Replogle and J. A. Pople, GAUSSIAN 98, Revision A.7, Gaussian, Inc., Pittsburgh PA, 1998.

30 A. Frish and M. J. Frisch, GAUSSIAN 98, User's Reference, Gaussian, Inc., Carnegie Office Park, Building 6, Pittsburgh, PA 15106, 2nd edn., 1998.

31 D. F. Shriver and P. W. Atkins, *Inorganic Chemistry*, Oxford University Press, Oxford, 3rd edn, 1999; and references therein.

32 D. Cremer and J. A. Pople, *J. Am. Chem. Soc.*, 1975, **97**, 1354.

33 (*a*) P. Luger, K. Daneck, W. Engel, G. Trummlitz and K. Wagner, *Eur. J. Pharm. Sci.*, 1996, **4**, 175; (*b*) G. F. Fabiola, V. Pattabhi, S. G. Manjunatha, G. V. Rao and K. Nagarajan, *Acta Crystallogr., Sect. C*, 1998, **54**, 2001.

34 (*a*) V. Scheller-Krattiger, K. H. Scheller, E. Sinn and R. B. Martin, *Inorg. Chim. Acta*, 1982, **60**, 45; (*b*) R. J. Anderson, P. H. Hagback and P. J. Steel, *Inorg. Chim. Acta*, 1999, **284**, 273.

35 S. Scheiner, *Hydrogen Bonding, A Theoretical Perspective*, Oxford University Press, Oxford, 1997.